Localized glucose and water influx facilitates *Cryptosporidium parvum* cellular invasion by means of modulation of host-cell membrane protrusion

Xian-Ming Chen, Steven P. O'Hara, Bing Q. Huang, Patrick L. Splinter, Jeremy B. Nelson, and Nicholas F. LaRusso*

Center for Basic Research in Digestive Diseases, Division of Gastroenterology and Hepatology, Mayo Clinic College of Medicine, Rochester, MN 55905

Edited by Peter C. Agre, The Johns Hopkins University School of Medicine, Baltimore, MD, and approved March 14, 2005 (received for review November 17, 2004)

Dynamic membrane protrusions such as lamellipodia and filopodia are driven by actin polymerization and often hijacked by intracellular microbes to enter host cells. The overall rate of membrane protrusion depends on the actin polymerization rate and the increase of localized cell volume. Although the signaling pathways involving actin polymerization are well characterized, the molecular mechanisms regulating local cell volume associated with membrane protrusion are unclear. *Cryptosporidium parvum*, an intracellular parasite, depends on host-cell membrane protrusion to accomplish cell entry and form the parasitophorous vacuole. Here, we report that *C. parvum* infection of cholangiocytes recruits host-cell SGLT1, a Na^+/glucose cotransporter, and aquaporin 1 (AQP1), a water channel, to the attachment site. SGLT1-dependent glucose uptake occurs at the attachment site. Concordantly, the region of attachment displays localized water influx that is inhibited by either suppression of AQP1 by means of AQP1-small interfering RNA (siRNA) or inhibition of SGLT1 by a specific pharmacologic inhibitor, phlorizin. Inhibition of SGLT1 does not affect actin accumulation but decreases the membrane protrusion at the attachment site. Moreover, functional inhibition of host-cell AQP1 and SGLT1 hampers *C. parvum* invasion of cholangiocytes. Thus, glucose-driven, AQP-mediated localized water influx is involved in the membrane protrusion during *C. parvum* cellular invasion, phenomena that may also be relevant to the mechanisms of cell membrane protrusion in general.

actin | aquaporin | cryptosporidiosis | Na^+/glucose cotransporter 1 | bile ducts

Localized membrane protrusions are crucial to numerous cell functions, including cell migration, neurite outgrowth, phagocytosis, and formation of cell–cell junctions (1–3). Many intracellular microbes also hijack the machinery of membrane protrusion to enter their host cells (4). Actin polymerization is essential for the formation and maintenance of membrane protrusions (1–3, 5). Actin filaments are assembled and organized as a dendritic network by actions of actin-associated signal pathways [such as Wiskott–Aldrich syndrome protein (WASP)/Arp 2/3 complex] that stimulate nucleation and branching of actin filaments. As a branched network of actin filaments grows by actin assembly at the barbed ends, the membrane is forced forward (1, 5). The overall rate of membrane protrusion depends not only on the rate of actin polymerization but also on an increase of localized cell volume. Cells regulate their volumes primarily by adjusting membrane permeability to water and ions (6). Aquaporins (AQPs) are channels specific for water and other small nonionic molecules (7). In response to gradients established by transport of osmotically active molecules across cell membranes, AQPs permit water to rapidly cross the plasma membranes of a wide variety of cell types (8), including cholangiocytes, the epithelial cells that line intrahepatic bile ducts (9). An important role of AQP1 has been reported for water transport by cholangiocytes, particularly water movement across the apical membrane in response to osmotic gradients generated by apical transporters/exchangers, such as the cystic fibrosis transmembrane regulator (CFTR) and the Na^+/glucose cotransporter 1 (SGLT1) (9–11). Moreover, AQP9 has been reported to be recruited to the motile regions of neutrophil leukocytes (12). Whether AQP-mediated water movement plays a role in cell membrane protrusion is unclear.

Cryptosporidium parvum, an intracellular parasite within the protist phylum Apicomplexa, infects gastrointestinal epithelia and other mucosal surfaces in humans, causing self-limited diarrhea in immunocompetent subjects and potentially life-threatening syndromes in immunocompromised individuals, primarily those with AIDS (13). Once ingested, *C. parvum* oocysts excyst in the gastrointestinal tract, releasing infective sporozoites. Mediated by poorly characterized but specific ligands on the sporozoite surface and unidentified receptors on the host cell, the sporozoite attaches to the apical membrane of the epithelial cell, inducing host-cell membrane protrusion that encapsulates the parasite in a parasitophorous vacuole (14–16). The parasite is then retained on the apical surface of the cell, and a unique "electron-dense band" of unknown composition is established that separates the organism from the host-cell cytoplasm and may facilitate the uptake of nutrients from the host. Thus, the parasitophorous vacuole membrane and dense band keep the internalized parasite intracellular but extracytoplasmic (14–16). Despite intensive efforts over the past decades, there is currently no effective therapy for cryptosporidiosis in humans (17).

Host-cell membrane protrusion plays an active role in *C. parvum* entry of epithelial cells. Inhibition of host-cell actin polymerization by pharmacological inhibitors, such as cytochalasin B and cytochalasin D (18, 19), or by cellular expression of specific inhibitory fragments of actin-associated proteins, such as Scar-WA (20), blocks *C. parvum* cellular invasion. Several intracellular signaling pathways are involved in *C. parvum*-induced actin polymerization, including the c-Src/cortactin and phosphatidylinositol 3-kinase (PI3-K)/Cdc42 pathways (21–23). Functional inhibition of those actin-associated signal pathways results in an inhibition of host-cell membrane protrusion and, subsequently, of parasite cellular invasion (21–23).

In work described here, we found that *C. parvum* recruits host-cell AQP1 and SGLT1 to the attachment site during *C. parvum* infection of cultured cholangiocytes. Recruitment of SGLT1 and AQP1 results in a localized increase of glucose uptake and a subsequent AQP1-mediated water influx at the attachment site. The localized water influx seems to enhance *C. parvum*-induced host-cell membrane protrusion and thus facilitates parasite cellular invasion. Thus, localized glucose-driven, AQP-mediated water influx is involved in membrane protrusion during *C. parvum* invasion,

This paper was submitted directly (Track II) to the PNAS office.

Abbreviations: SGLT1, Na^+/glucose cotransporter 1; AQP, aquaporin; 2-NBDG, 2-[*N*-(7-nitrobenz-2-oxa-1,3-diazol-4-yl) amino]-2-deoxy-glucose; siRNA, small interfering RNA; calcein-AM, calcein-acetoxymethyl ester.

*To whom correspondence should be addressed. E-mail: larusso.nicholas@mayo.edu.

www.pnas.org/cgi/doi/10.1073/pnas.0408563102

a phenomenon that is also relevant to the general mechanisms of cell membrane protrusion.

Materials and Methods

***C. parvum* and Cholangiocyte Cell Lines.** *C. parvum* oocysts of the Iowa strain were purchased from a commercial source (Bunch Grass Farm, Deary, ID). H69 cells (a gift of D. Jefferson, Tufts University, Medford, MA) are SV40-transformed normal human cholangiocytes (24). 603B cells are immortalized normal mouse cholangiocytes (a gift from Y. Ueno, Tohoku University School of Medicine, Sendai, Japan) (25).

***In Vitro* Models and Infection Assay.** An attachment model and an attachment/invasion model were used as described (18). Before infecting cells, oocysts were excysted to release infective sporozoites (18). Infection was done in a culture medium consisting of DMEM-F12, 100 units/ml penicillin, 100 μg/ml streptomycin, and freshly excysted sporozoites (1×10^6 sporozoites per slide well or culture plate). Inactivated organisms (treated at 65°C for 30 min) were used for sham infection controls. Infection assays (attachment rate or attachment/invasion rate) were carried out after incubation of 1 h with the parasite employing an indirect immunofluorescent approach (18). Briefly, the number of parasites and cells was counted randomly in each group, and results were expressed as attachment or attachment/invasion rate [(the number of parasites per total number of cells) $\times$ 100]. A total of >2,000 cells were counted for each slide, and all assays were performed in triplicate. For the inhibitory experiments, one specific inhibitor of SGLT1, phlorizin (26), was added in the medium at the same time as *C. parvum*. A concentration of 0.2 μM phlorizin, which showed no cytotoxic effects on 603B cells or on *C. parvum* sporozoites, was selected for the study.

AQP1-Small Interfering RNA (siRNA) and Plasmid Constructs. Generation of AQP1-siRNA and subsequent suppression of AQP1 expression have been described (27). A nonspecific siRNA containing the same nucleotides but in irregular sequence (i.e., scrambled siRNA) was used as the control. The AQP1-siRNA was labeled with Cy3 by using the Silencer siRNA labeling kit (Ambion, Austin, TX). Cells were transfected with AQP1-siRNA by using the si-PORT lipid transfection agent (Ambion). pEGFP-N1-AQP1 was generated by inserting the complete rat AQP1 into the expression vector pEGFP-N1 (Invitrogen). The pEGFP-N1 empty vector and pEGFP-N1-GFP-Dynamin2 (a gift of M. A. McNiven, Mayo Clinic College of Medicine) were used as the controls. Cells were transfected with GFP constructs with the Lipofectamine Plus reagent kit (Ambion). Twenty-four hours after transfection, cells were exposed to *C. parvum* sporozoites.

Immunofluorescent Microscopy. After exposure to *C. parvum* as described above, cells were fixed with 2% paraformaldehyde and permeabilized with 0.2% (vol/vol) Triton X-100 in PBS. For double-immunofluorescent labeling, fixed cells were incubated with primary antibodies to associated proteins mixed with antibodies against *C. parvum*, followed by anti-mouse and anti-rabbit secondary antibodies (Molecular Probes) by using the standard costaining approach. A polyclonal antibody against *C. parvum* sporozoite proteins (28) (a gift from Guan Zhu and Janet Keithly, Wadsworth Center, Albany, NY) and a monoclonal antibody to *C. parvum* sporozoite (2H2, ImmuCell, Portland, ME) were used to label the parasite. To confirm the specificity of AQP1 and SGLT1 staining, two antibodies against AQP1 (clone B8 antibody from Santa Cruz Biotechnology and a polyclonal antibody from Calbiochem) and two antibodies to SGLT1 (Upstate Biotechnology, Lake Placid, NY) were used. For localization of actin with *C. parvum*, rhodamine-phalloidin (Cytoskeleton, Denver) was coincubated with the secondary antibody. In some experiments, DAPI (5 μM) was used to stain cell nuclei. Labeled cells were assessed by confocal laser scanning microscopy.

Visualization of Glucose Uptake. A fluorescent glucose analogue, 2-[*N*-(7-nitrobenz-2-oxa-1,3-diazol-4-yl) amino]-2-deoxy-glucose (2-NBDG) (Molecular Probes), was used to measure localized glucose uptake in single cells (29). Briefly, 603B cells were grown on cover-glass-bottomed 3-cm dishes to subconfluence. Cells were then exposed to freshly excysted *C. parvum* sporozoites in the infection medium containing 1% glucose with or without 0.2 μM phlorizin for 50 min at 37°C. 2-NBDG was then added to the culture medium (at a final concentration of 200 μM). 2-NBD, a control probe provided by the manufacturer (Molecular Probes), was also used. After incubation at 37°C for 10 min, cells were assessed by real-time confocal microscopy. Fluorescence intensity at 520–560 nm wavelength (excitation wavelength 488 nm) was measured and calculated with an analysis system of the LSM 510 provided by Carl Zeiss. A total of 500 parasite attachment sites were randomly selected and measured for each condition. Results represent three independent experiments.

Visualization of Sites with Water Influx. A calcein fluorescence quenching method was used to assess the water influx as described (12. 30). A water influx changes the cytosolic protein concentration in the region and thus alters calcein quenching, resulting in an increase of calcein fluorescence (30). Briefly, 603B cells were grown on cover-glass-bottomed 3-cm dishes to subconfluence. Cells were then exposed to the infection medium containing 10 μM calcein-acetoxymethyl ester (calcein-AM, Molecular Probes) at 37°C for 30 min. After extensive washing with culture medium, cells were then exposed to freshly excysted *C. parvum* sporozoites for 1 h at 37°C, followed by real-time confocal microscopy as described above.

Electron Microscopy. For scanning electron microscopy (SEM) and transmission electron microscopy (TEM), cells were prepared as described in the product literature (Technical Bulletins 405 and 406, Electron Microscopy Sciences, Hatfield, PA). The length of membrane protrusions was determined by measuring the distance from tip to base on digitized TEM images. A total of ≈200 parasite attachment sites were measured for each condition, and results represent three independent experiments. For immunogold labeling, cells were fixed and processed according to the protocol as described (21, 22). The relative distribution of AQP1 was determined by counting gold particles over cell profiles. Dense-band and parasitophorous vacuole membrane-associated labeling was quantitated by counting the gold particles in the area within a 0.2-μm distance along the dense-band or vacuole membrane; totals were described as gold particles per μm^2. Gold particles at randomly selected cytoplasm and apical membrane areas (within a 0.2-μm distance along membrane surface) were also counted in both sham and *C. parvum*-infected cells. A total of ≈100 parasite attachment sites and >2,000 gold particles were counted randomly for each condition; data represent three independent experiments.

Results

***C. parvum* Recruits Cholangiocyte AQP1 to the Attachment Sites.** We chose two cell lines for the study: 603B cells, which express endogenous AQP1, and H69 cells, which don't express endogenous AQP1 as confirmed by both Western blotting and immunofluorescent staining (data not shown). When 603B cells were exposed to *C. parvum*, very strong staining of AQP1 was observed at the attachment site by immunofluorescence (Fig. 1*A*). No accumulation of AQP1 was detected in sham-infected control cells, and no positive staining of AQP1 was found in the parasite itself (data not shown). To confirm the host-cell origin of AQP1, we transfected a GFP-AQP1 construct into H69 cells and then exposed the cells to *C. parvum*. A similar expression pattern of AQP1-GFP was found in transfected H69 cells compared with the antibody staining in

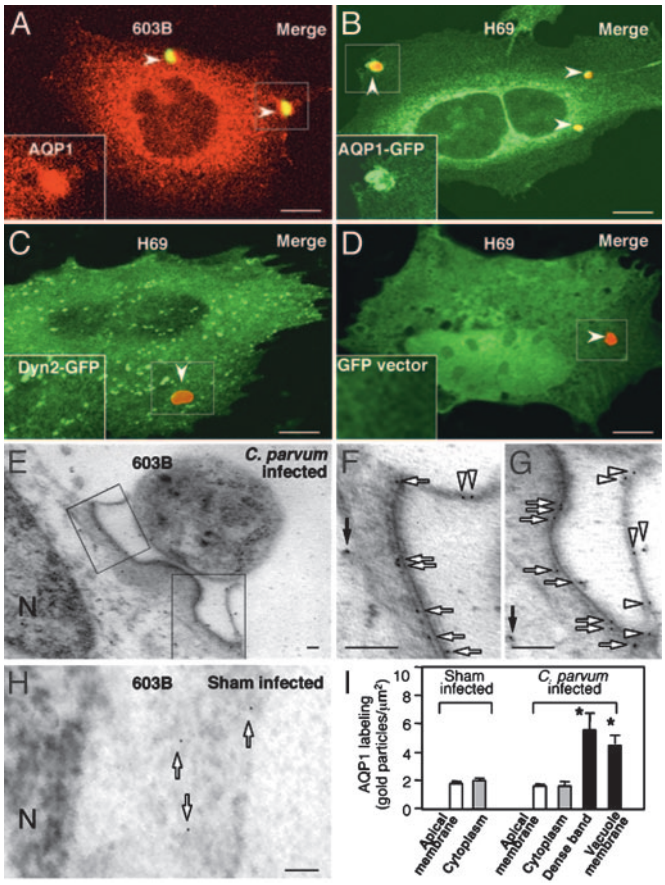

Fig. 1. *C. parvum* recruits cholangiocyte AQP1 to the attachment site. (*A*) Strong staining of AQP1 (in red) was detected by dual immunofluorescent staining at the attachment site in 603B cells (arrowheads). (*B*) Recruitment of GFP-AQP1 to the attachment site (arrowheads) in H69 cells transfected with a GFP-AQP1 construct. (*C* and *D*) No accumulation of GFP fluorescence was found at the attachment site in cells transfected with the GFP-dynamin 2 (arrowhead in *C*) and the GFP-empty vector (arrowhead in *D*). (*A–D Insets*) Higher magnifications of the boxed regions showing AQP1 (*A*) or GFP fluorescence (*B–D*). (*E*) Immunogold labeling of AQP1 at the parasite–host cell interface in 603B cells. (*F* and *G*) Higher magnifications of the boxed regions in *E*. Accumulations of gold particles were found along the dense-band (arrows) or at the parasitophorous vacuole membrane (arrowheads). (*H*) Immunogold labeling of AQP1 in sham-infected cells. (*I*) Quantitative analysis of immunogold particles for AQP1. Each data bar represents mean ± SE. *, $P < 0.05$, ANOVA vs. apical membrane labeling. Dyn2, dynamin 2; N, nucleus. (Scale bars: 2 μm in *A–D* and 0.1 μm in *E–H*.)

603B cells, and a strong accumulation of GFP-AQP1 was found at the attachment site (Fig. 1*B*). In contrast, no accumulation of fluorescence was found at the parasite attachment sites in cells transfected with the GFP-dynamin 2 (Fig. 1*C*), a GFP fusion protein that is not associated with *C. parvum* cellular invasion (21), and the GFP empty vector (Fig. 1*D*). To further localize the accumulation of AQP1 in infected cells, 603B cells exposed to *C. parvum* sporozoites were assessed by immuno-electron microscopy by using an antibody to AQP1. Colloidal gold particles specific for AQP1 accumulated along the dense-band region. Some labeling was also observed at the parasitophorous vacuole membrane (Fig. 1 E–G), whereas fewer gold particles were found in the cytoplasm not directly adjacent to the parasite in infected cells (solid arrow in Fig. 1*F*). Sham-infected cells showed no membrane accumulation of gold particles but a scattered distribution in the cytoplasm (arrows in Fig. 1*H*). Quantitative analysis showed a significant increase of gold particles for AQP1 along the dense-band and at the parasitophorous vacuole membrane compared with other areas not directly adjacent to the parasite or in sham infection controls (Fig. 1*I*).

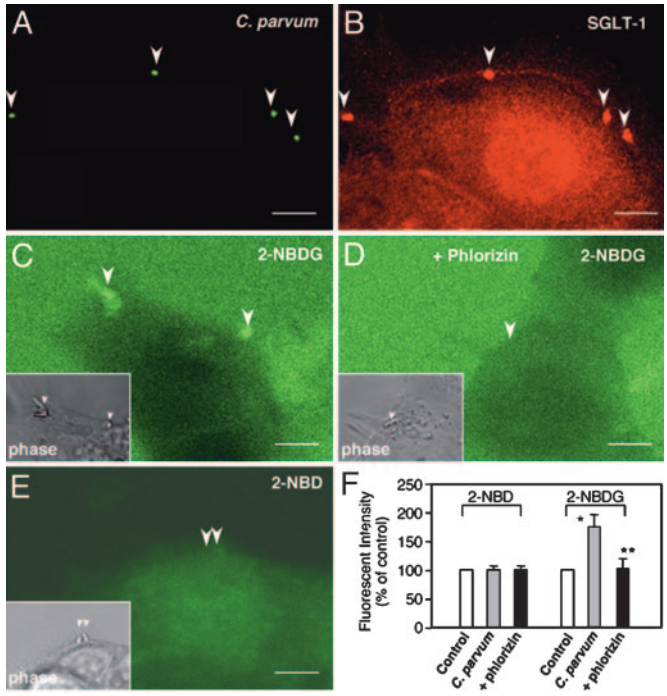

Fig. 2. *C. parvum* recruits cholangiocyte SGLT1 to the attachment site and induces a localized glucose uptake in 603B cells. (*A* and *B*) Representative confocal micrographs showing accumulation of SGLT1 at the attachment site. (*C*) A representative real-time confocal micrograph showing an increased uptake of 2-NBDG at the attachment site (arrowheads). (*D*) No increase of 2-NBDG fluorescence at the attachment site was observed in the presence of phlorizin (arrowhead). (*E*) No increase of fluorescence for the control probe, 2-NBD, was found at the attachment site (arrowhead). (*C–E Insets*) The phase images of the same fields showing the parasite (arrowheads) in *C–E*. (*F*) Quantitative analysis of 2-NBD and 2-NBDG uptake at the attachment site. *, $P < 0.05$, ANOVA, *C. parvum* vs. control (fluorescence at the nearby region); **, $P < 0.05$ vs. *C. parvum*. (Scale bars: 5 μm.)

***C. parvum* Recruits Cholangiocyte SGLT1 to the Attachment Sites and Induces a Localized Glucose Uptake.** 603B cells were exposed to *C. parvum* followed by immunofluorescent labeling for SGLT1, a Na^+/glucose cotransporter on the apical membrane domain. Strong staining of SGLT1 was observed at the *C. parvum* attachment site (arrowheads in Fig. 2 *A* and *B*). To test whether SGLT1 is activated, we used a real-time fluorescent-based approach using 2-NBDG, a fluorescent glucose analogue, to measure the uptake of glucose in infected cells. An increase of fluorescence was found at the *C. parvum* attachment site in 603B cells (Fig. 2*C*), and no increase of fluorescence was found over the parasite attachment site in the presence of phlorizin (Fig. 2*D*). No labeling of 2-NBDG was found in the parasite itself with the approach used (data not shown). Moreover, no increase of fluorescence to the control probe, 2-NBD, was found over the parasite attachment site (Fig. 2*E*). Quantitative analysis showed a marked increase of 2-NBDG fluorescent intensity at the attachment sites compared with other regions not directly adjacent to the parasite or in the presence of phlorizin (Fig. 2*F*).

***C. parvum* Induces an SGLT1 and APQ1-Dependent Water Influx at the Attachment Sites.** To test whether AQP1 accumulation facilitates water movement across the plasma membrane, we measured water movement in infected cells by using a calcein fluorescence quench-

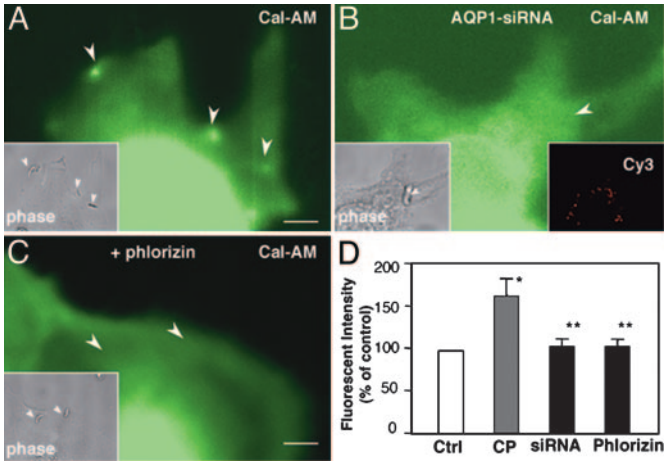

Fig. 3. *C. parvum* induces a SGLT1 and APQ1-dependent water influx at the attachment site in 603B cells. (*A*) A representative real-time confocal micrograph showing a localized water influx at the attachment site. Increase of fluorescence for calcein-AM was detected at attachment site (arrowheads). (*B*) Inhibition of water influx at the attachment site (arrowhead) in cells transfected with Cy3-tagged AQP1-siRNA. (*Right Inset*) Cy3 panel. (*C*) No increase of calcein-AM fluorescence at the attachment site was detected in the presence of phlorizin (arrowheads). (*A–C Insets*) The phase images of the same corresponding fields showing the parasite (arrowheads). (*D*) Quantitative analysis of calcein-AM fluorescent intensities at the attachment site. *, $P <$ 0.05 ANOVA, *C. parvum* (CP) vs. control (Ctrl, fluorescence at the nearby region); **, $P < 0.05$ vs. CP. (Scale bars: 5 μm.)

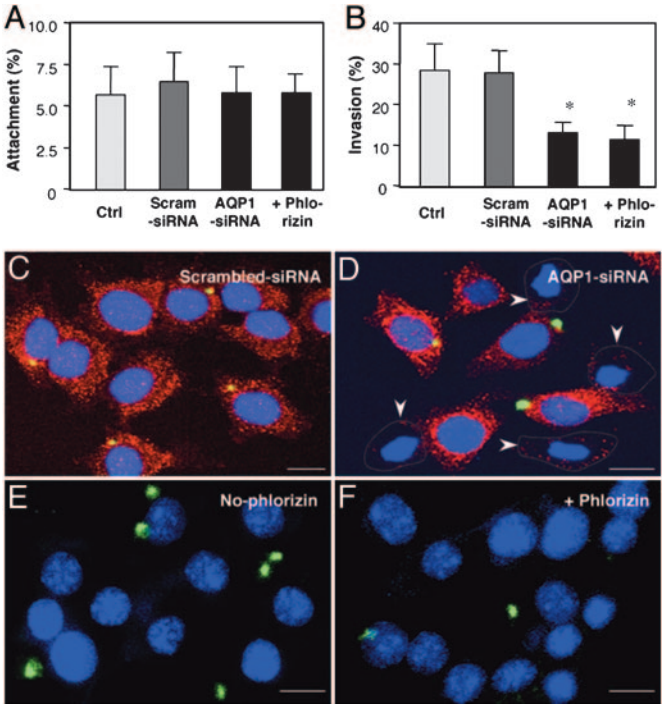

Fig. 4. Inhibition of AQP1 and SGLT1 hampers *C. parvum* invasion. 603B cells were either exposed to *C. parvum* in the presence of phlorizin or transfected with either AQP1-siRNA or scrambled siRNA and then exposed to *C. parvum* for 1 h. (*A*) Attachment assay in prefixed cells. (*B*) Attachment/invasion assay in nonprefixed cells. (*C* and *D*) Representative confocal images of attachment/invasion of *C. parvum* by nonprefixed cells treated with scrambled siRNA (*C*) or AQP1-siRNA (*D*). (*E* and *F*) Representative confocal images of attachment/invasion of *C. parvum* by nonprefixed cells in the absence (*E*) or presence (*F*) of phlorizin. *, $P < 0.05$, *t* test vs. nontreatment control (Ctrl) or scrambled siRNA. (Scale bars: 5 μm.)

ing approach. Strong fluorescence was observed at the attachment site in infected 603B cells (Fig. 3*A*), reflecting localized water influx (30). No labeling of calcein-AM was found in the parasite itself with the approach used (data not shown). To test whether the localized water influx at the attachment site is AQP1-mediated, we first transfected 603B cells with Cy3-tagged AQP1-siRNA to suppress AQP1 expression and then measured water influx at the attachment site in infected cells after exposure to *C. parvum*. As shown in Fig. 3*B*, no obvious increase of fluorescence was found at the attachment site in siRNA-transfected 603B cells.

To test whether SGLT1-associated glucose uptake is associated with *C. parvum*-induced AQP1-mediated localized water influx, we tested the effect of phlorizin on *C. parvum*-induced water influx. As shown in Fig. 3*C*, no obvious increase of calcein-AM fluorescence was found at the attachment site in the presence of phlorizin. Quantitative analysis showed: (*i*) a significant increase of water influx-associated fluorescent intensity at the attachment site in 603B cells (Fig. 3*D*); and (*ii*) a significant decrease of water influx-associated fluorescent intensity at the attachment site in 603B cells in the presence of phlorizin or in cells transfected with AQP1-siRNA (Fig. 3*D*).

Functional Manipulation of AQP1 and SGLT1 Affects *C. parvum* Invasion of Cholangiocytes. To further determine whether accumulation of AQP1 and SGLT1 and subsequent water influx are involved in parasite cellular invasion, we manipulated the function of AQP1 and SGLT1 in host cells and tested the effects on *C. parvum* invasion. 603B cells were first transfected with AQP1-siRNA and, 24 h later, exposed to *C. parvum*. Phlorizin was also used to test the role of SGLT1 in *C. parvum* entry of host cells. When cholangiocytes were prefixed and then exposed to *C. parvum* sporozoites, a model in which the organism can attach only to the fixed cells, no significant change of attachment rate was found among all experimentally manipulated cells (Fig. 4*A*); these results suggest that *C. parvum* sporozoite attachment to cholangiocytes is not dependent upon host-cell AQP1 and SGLT1. In contrast, when unfixed living cells were exposed to *C. parvum* sporozoites, a model in which the organism can both attach to and enter into host cells, significantly fewer parasites were detected in cells transfected with AQP1-siRNA or in the presence of phlorizin (Fig. 4*B*). Transfection of cells with a scrambled siRNA did not show any effect on *C. parvum* attachment or invasion. Representative confocal images showing inhibition of *C. parvum* invasion of unfixed cells transfected with AQP1-siRNA or in the presence of phlorizin are shown in Fig. 4 *C–F*.

Because decrease of AQP1 expression hampers *C. parvum* cellular invasion in 603B cells, we predicted that up-regulation of AQP1 could increase *C. parvum* entry of host cells. To test this possibility, we overexpressed a functional GFP-AQP1 construct in H69 cells and then exposed them to *C. parvum* for 1 h. Although no difference in attachment rate was found between prefixed transfected cells and nontransfected cells, significantly more parasites were found in unfixed transfected cells compared with nontransfected cells (Fig. 5 *A* and *B*). A representative confocal image of unfixed cells is shown in Fig. 5*C*.

Inhibition of SGLT1 by Phlorizin Does Not Affect Localized Actin Accumulation but Hampers *C. parvum*-Induced Cholangiocyte Membrane Protrusion. To test how SGLT1, as well as subsequent AQP1-mediated water influx, affects *C. parvum* cellular invasion, we observed host-cell actin accumulation and membrane protrusion in 603B cells during *C. parvum* invasion in the presence or absence of phlorizin by confocal microscopy and electron microscopy. Phalloidin, which binds to host-cell F-actin but not *C. parvum* actin (19), revealed accumulation of actin at the attachment sites both in the presence and absence of phlorizin (Fig. 6 *A* and *B*). In the absence of phlorizin, cells showed obvious membrane protru-

CELL BIOLOGY

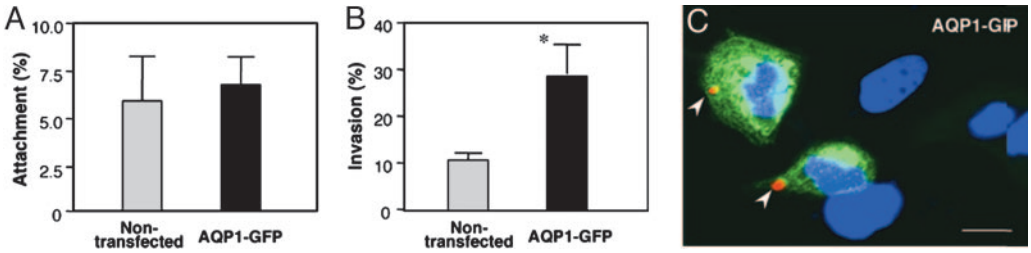

Fig. 5. Expression of AQP1 in H69 cells increases *C. parvum* invasion. H69 cells were transfected with a AQP1-GFP construct for 24 h and then exposed to *C. parvum* for 1 h. (*A*) Attachment assay in prefixed cells. (*B*) Attachment/invasion assay in nonprefixed cells. (*C*) A representative confocal image of attachment/invasion of *C. parvum* (arrowheads) by nonprefixed cell culture transfected with the AQP1-GFP construct. Cells transfected with AQP1-GFP were identified with the GFP expression. *, $P < 0.05$, *t* test. (Scale bar: 5 μm.)

sion enveloping the organism at the parasite attachment site (arrowheads in Fig. 6*C*). In contrast, much less host-cell membrane protrusion was found in the presence of phlorizin (arrowhead in Fig. 6*D*). Quantitative analysis showed a significant decrease of length of membrane protrusions at the attachment site in 603B cells in the presence of phlorizin compared with the controls (Fig. 6*E*).

Discussion

The key findings in this report are as follows: (*i*) *C. parvum* infection of cholangiocytes recruits host-cell SGLT1 and AQP1 to the attachment site, resulting in a localized increase of active glucose uptake by SGLT1 and subsequent passive water influx by means of AQP1; and (*ii*) localized glucose and water influx seem to be involved in host-cell membrane protrusion and subsequent parasite cellular invasion. Thus, *C. parvum* recruits host-cell SGLT1 and AQP1 to the attachment site, generating a localized water influx, thereby facilitating parasitic cellular invasion by means of modulation of host-cell membrane protrusion.

Cellular invasion by *C. parvum* is characterized by the formation of a tunnel connection between the anterior vacuole in the apical region of the sporozoite and the host-cell cytoplasm (31) and by host-cell membrane protrusion to encapsulate the invading parasite. At the base of each vacuole, a unique "electron-dense band" is established (13–16). A variety of molecules from both the parasite and the host cell accumulate at the host–parasite interface, including CpABC, a recently identified *C. parvum* ATP-binding cassette protein (32), and various host-cell actin-associated proteins, such as cortactin (21) and Cdc42 (22). It has been postulated that recruitment of transporters/exchangers/channels to the host–parasite boundary can supply the parasite with various nutritional requirements (14). Here, we have shown that *C. parvum* infection of cholangiocytes recruits host-cell SGLT1 and AQP1 to the attachment site. Accumulation of AQP1 was found both at the parasitophorous vacuole membrane and along the dense band region. Interestingly, functional inhibition of host-cell SGLT1 by a specific inhibitor, phlorizin, or suppression of AQP1 expression in host cells by a specific AQP1-siRNA, significantly decreased parasite cellular invasion. In addition, overexpression of a GFP-AQP1 construct in H69 cells increased *C. parvum* cellular invasion. Thus, it seems that, during the early infection stage, *C. parvum* recruits host-cell SGLT1 and AQP1 to the attachment site, a process that is directly associated with parasitic cellular invasion.

Cellular invasion by *C. parvum* depends on host-cell actin polymerization and subsequent membrane protrusion at the host–parasite interface. Inhibition of host-cell actin polymerization inhibits *C. parvum*-induced membrane protrusion and reduces parasite cellular invasion (18–20). We found that inhibition of SGLT1 did not affect actin-accumulation at the host–parasite interface. Instead, we detected a localized increase of glucose uptake at the attachment site during *C. parvum* invasion. A specific inhibitor of SGLT1, phlorizin, completely blocked glucose uptake by 603B cells. Cells loaded with calcein-AM displayed an increase

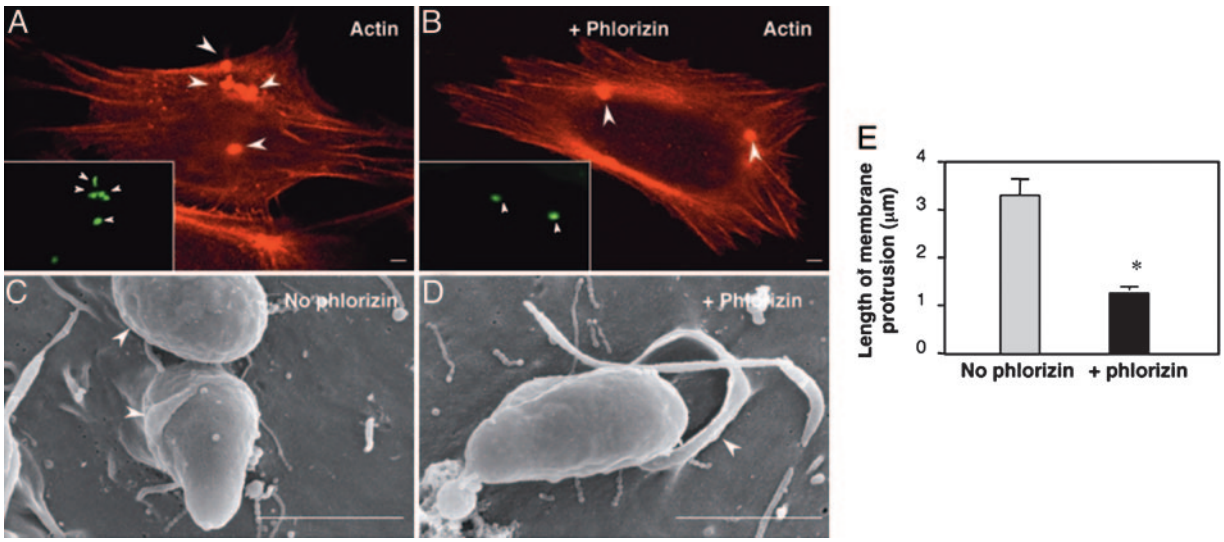

Fig. 6. Inhibition of SGLT1 by phlorizin does not affect localized actin accumulation but hampers *C. parvum*-induced cholangiocyte membrane protrusion in 603B cells. (*A* and *B*) Strong actin accumulation was found at the attachment site both in the absence (*A*) and presence (*B*) of phlorizin. (*C* and *D*) Host-cell membrane protrusion at the parasite–host interface as assessed by scanning electron microscopy (SEM). (*E*) Quantitative analysis of length of membrane protrusion based on transmission electron microscopy (TEM) images. *, $P < 0.05$, *t* test. (Scale bars: 1 μm.)

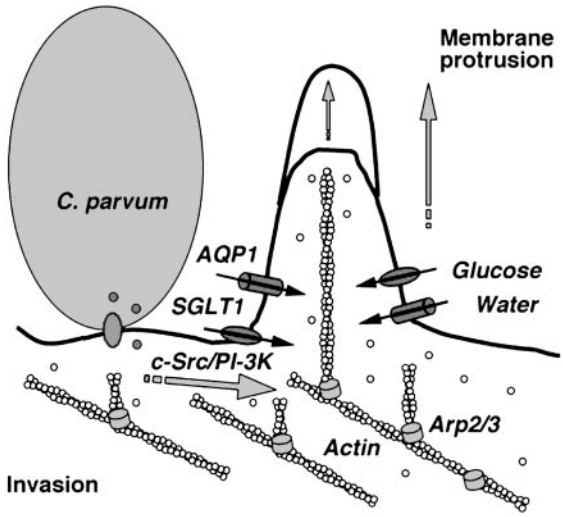

Fig. 7. *C. parvum* attachment to host-cell membrane activates c-Src/PI-3K pathways to induce actin remodeling at the parasite-attachment site. *C. parvum* also recruits host-cell SGLT1 and AQP1 to the attachment site and generates a localized water influx. This localized water influx facilitates membrane protrusion and thus benefits *C. parvum* cellular invasion.

of fluorescence at *C. parvum* attachment sites compared with nearby regions, suggesting localized water influx (30). Inhibition of either SGLT1 or AQP1 blocked the localized water influx, indicating that the water-influx is AQP1-mediated and likely requires the osmotic gradient generated by the uptake of glucose by means of SGLT1. Moreover, inhibition of SGLT1 by phlorizin significantly hampered *C. parvum*-induced cholangiocyte membrane protrusion as assessed by electric microscopy. Therefore, we postulated that *C. parvum* recruits host-cell SGLT1 and AQP1 to the attachment site, generating a glucose-driven localized inward osmotic gradient followed by regional influx of water, processes that facilitate the localized host-cell membrane protrusion required for parasitic cellular invasion.

Pollard and Borisy (1) have recently depicted the dendritic-nucleation model to explain the formation of membrane protrusions based on actin polymerization. It proposes that actin filaments growing by actin assembly at the barbed ends produce enough force to push the plasma membrane outward. What this model does not address is how cells quickly accommodate the resultant increase of localized cell volume accompanying membrane protrusion. Cells regulate their volume mainly by means of water and ion transport, and AQPs are water channels that allow rapid passive water movement across membranes in response to gradients established by the transport of osmotically active molecules such as glucose (7, 8). Our data support the notion that *C. parvum* recruits functionally active host-cell SGLT1 to the attachment site to induce a localized uptake of glucose, generating an inward osmotic gradient to drive regional inward water movement by means of AQP1. AQP1-mediated localized water influx accommodates the increase of cell volume accompanying localized membrane protrusion, facilitating *C. parvum* cellular invasion.

Loitto *et al.* (12) recently reported that AQP9 is recruited to the motile regions of neutrophil leukocytes. It has been postulated that, during membrane protrusion, localized water influx generates a gap between the filament ends and the membrane, thereby allowing for rapid polymerization of actin. Thus, a regulated water influx will allow for gel-to-sol transitions, osmotic forces, and subsequent dendritic nucleation, indicating that AQPs may be involved in the regulation of water movement in a localized region such as membrane protrusion. Coupling our current and previous studies with the work of others, the results suggest that *C. parvum* activates host-cell intracellular signaling pathways to induce actin polymerization at the attachment site, generating a force for membrane protrusion. *C. parvum* also recruits host-cell SGLT1 and AQP1 to the attachment site, generating localized glucose and water influx to accommodate the increase of cell volume accompanying membrane protrusion. Actin polymerization and rapid increase of local cell volume result in efficient localized membrane protrusion, thereby facilitating parasite cellular invasion (Fig. 7).

In conclusion, our data indicate that a pathogen, *C. parvum*, recruits host-cell SGLT1 and AQP1 to the attachment site, generating localized glucose and water influx that are required for efficient membrane protrusion and parasite invasion. It will be of interest to extend these studies to determine the mechanisms by which *C. parvum* recruits SGLT1 and AQP1 to the attachment site. Our studies not only provide insight into the mechanism of *C. parvum* entry of host epithelial cells, but also are relevant to the general molecular mechanisms of cell membrane protrusion.

We thank Drs. M. A. McNiven and A. I. Masyuk and Ms. P. A. Tietz for helpful and stimulating discussions and Ms. D. Hintz for secretarial assistance. This work was supported by National Institutes of Health Grants DK57993 and DK24031 and by the Mayo Foundation.

1. Pollard, T. D. & Borisy, G. G. (2003) *Cell* **112,** 453–465.
2. Ridley, A. J., Schwartz, M. A., Burridge, K., Firtel, R. A., Ginsberg, M. H., Borisy, G., Parsons, J. T. & Horwitz, A. R. (2003) *Science* **302,** 1704–1709.
3. Ridley, A. J. (2003) *Cell* **116,** 357–358.
4. Finlay, B. B. & Cossart, P. (1997) *Science* **276,** 718–725.
5. DeMali, K. A. & Burridge, K. (2003) *J. Cell Sci.* **116,** 2389–2397.
6. Lang, F., Busch, G. L., Ritter, M., Volkl, H., Waldegger, S., Gulbins, E. & Haussinger, D. (1998) *Physiol. Rev.* **78,** 247–306.
7. Agre, P., King, L. S., Yasui, M., Guggino, W. B., Ottersen, O. P., Fujiyoshi, Y., Engel, A. & Nielsen, S. (2002) *J. Physiol. (London)* **542,** 3–16.
8. Verkman, A. S. & Mitra, A. K. (2000) *Am. J. Physiol.* **278,** F13–F28.
9. Marinelli, R. A., Pham, L. D., Agre, P. & LaRusso, N. F. (1997) *J. Biol. Chem.* **272,** 12984–12988.
10. Marinelli, R. A., Tietz, P. S., Pham, L. D., Rueckert, L., Agre, P. & LaRusso, N. F. (1999) *Am. J. Physiol.* **276,** G280–G286.
11. Tietz, P. S., Marinelli, R. A., Chen, X. M., Huang, B., Cohn, J., Kole, J., McNiven, M. A., Alper, S. & LaRusso, N. F. (2003) *J. Biol. Chem.* **278,** 20413–20419.
12. Loitto, V. M., Forslund, T., Sundqvist, T., Magnusson, K. E. & Gustafsson, M. (2002) *J. Leukocyte Biol.* **71,** 212–222.
13. Chen, X. M., Keithly, J. S., Paya, C. V. & LaRusso, N. F. (2002) *N. Engl. J. Med.* **346,** 1723–1731.
14. O'Donoghue, P. J. (1995) *Int. J. Parasitol.* **25,** 139–195.
15. Tzipori, S. & Griffiths, J. K. (1998) *Adv. Parasitol.* **40,** 5–36.
16. Clark, D. P. (1999) *Clin. Microbiol. Rev.* **12,** 554–563.
17. Mead, J. R. (2002) *Drug Resist. Updat.* **5,** 47–57.
18. Chen, X. M. & LaRusso, N. F. (2000) *Gastroenterology* **118,** 368–379.
19. Forney, J. R., DeWald, D. B., Yang, S., Speer, C. A. & Healey, M. C. (1999) *Infect. Immun.* **67,** 844–852.
20. Elliott, D. A. & Clark, D. P. (2000) *Infect. Immun.* **68,** 2315–2322.
21. Chen, X. M., Huang, B. Q., Splinter, P. L., Cao, H., Zhu, G., McNiven, M. A. & LaRusso, N. F. (2003) *Gastroenterology* **125,** 216–228.
22. Chen, X. M., Huang, B. Q., Splinter, P. L., Orth, J. D., Billadeau, D. D., McNiven, M. A. & LaRusso, N. F. (2004) *Infect. Immun.* **72,** 3011–3021.
23. Chen, X. M., Splinter, P. L., Tietz, P. S., Huang, B. Q., Billadeau D. D. & Larusso, N. F. (2004) *J. Biol. Chem.* **279,** 31671–31678.
24. Grubman, S. A., Perrone, R. D., Lee, D. W., Murray, S. L., Rogers, L. C., Wolkoff, L. I., Mulberg, A. E., Cherington, V. & Jefferson, D. M. (1994) *Am. J. Physiol.* **266,** G1060–G1070.
25. Handa, S., Harada, M., Koga, H., Kawaguchi, T., Taniguchi, E., Kumashiro, R., Ueno, T., Ueno, Y., Ishii, M., Sakisaka, S. & Sata, M. (2003) *Liver Int.* **23,** 3–11.
26. Briski, K. P. & Marshall, E. S. (2001) *Neurochem. Res.* **26,** 783–792.
27. Splinter, P. L., Masyuk, A. I. & LaRusso, N. F. (2002) *J. Biol. Chem.* **278,** 6268–6274.
28. Zhu, G., Marchewka, M. J., Woods, K. M., Upton, S. J. & Keithly, J. S. (2000) *Mol. Biochem. Parasitol.* **105,** 253–260.
29. Lloyd, P. G., Hardin, C. D. & Sturek, M. (1999) *Physiol. Res.* **48,** 401–410.
30. Solenov, E., Watanabe, H., Manley, G. T. & Verkman, A. S. (2004) *Am. J. Physiol.* **286,** C426–32.
31. Huang, B. Q., Chen, X. M. & LaRusso, N. F. (2004) *J. Parasitol.* **90,** 212–221.
32. Perkins, M. E., Riojas, Y. A., Wu, T. W. & Le Blancq, S. M. (1999) *Proc. Natl. Acad. Sci. USA* **96,** 5734–5739.